CORE-SHELL ELECTROSPUN CARBON NANOFIBER/SILICON NANOPARTICLE COMPOSITE FOR LITHIUM ION BATTERY APPLICATION

N. Lee[1], E. Fok[2], H. Yang[1], J. Madden[2], F. Ko[1]*
[1] Department of Materials Engineering, University of British Columbia, Vancouver, Canada, [2] Department of Electrical Engineering, University of British Columbia, Vancouver, Canada
* Corresponding author (frank.ko@ubc.ca)

Keywords: *carbon nanofiber, silicon nanoparticle, electrospinning, lithium*

1 Introduction

Rechargeable lithium ion batteries (LIB), known for its light weight, high energy density, and high voltage capacity per cell, possess a great potential in heavy duty hybrid electric vehicles, aerospace, and military applications [1]. Graphite is used in industry as a standard anode material due to its stable charge/discharge profile and a long plateau at 0.1 V vs. Li metal. However, its maximum theoretical capacity is limited to 372 mAh/g, corresponding to LiC_6 structure upon Li intercalation [2-4].

Much research has been devoted to increase the energy densities (both Wh/kg and Wh/L) of LIB. Hard carbons are used but the capacity has limited improvement [5]. Various alternative alloying metals have been investigated, among all, silicon is most promising due to its highest theoretical specific capacity of 4200 mAh/g by alloying with 4.4 Li atoms. It also possesses a low charge/discharge plateau at 0 – 0.4 V, which permits high energy output. However, the major challenge for Si-based anode is its 400% volume change during Li ion alloying/de-alloying. This often results in particle fusion, pulverization, and the loss of electrical contact of Si to the current collector [6-8]. Researchers are trying to reduce the amount of volume expansion and contraction by reducing the size of Si to nano-scale [9,10]. Carbon has demonstrated to be a suitable coating material for Si to prevent nanoparticle agglomeration upon volume expansion and to generate a stable solid electrolyte interface (SEI) for stable capacity [11].

In this study, a simple and scalable LIB anode fabrication method was demonstrated using electrospun carbon nanofiber (CNF) as the carrier matrix for silicon nanoparticles (SiNP). Core-shell electrospinning was conducted using Poly(acrylonitrile-co-acrylamide) (PANAM) as both the precursor for CNF and the carrier matrix for SiNP. The structural change of carbon at the addition of different amount of SiNP was analyzed. Its electrochemical behavior was also compared with non-core-shell CNF/Si nano-composite and pure CNF. This study demonstrated that core-shell electrospinning contains SiNP well within the carbon matrix, which prevents nanoparticle fusion, maintains a good electrical contact, and permits constant capacity for SiNP during charge/discharge.

2 Experimental

PANAM with an average viscosity molecular weight of 1.98×10^5 g/mol was synthesized using free radical polymerization. For core-shell electrospinning, a core solution of 8.5 wt% PANAM with 15, 30, 50, or 80 wt% SiNP in N,N-dimethylformamide (DMF) and a shell solution of 8.5 wt% PANAM in DMF were prepared and co-electrospun into non-woven composite nanofibers. Non-core-shell nanofibers were also prepared by electrospinning a DMF solution composed of 9 wt% PANAM/30 wt% SiNP. Pure PANAM nanofiber was prepared by electrospinning 10 wt% PANAM in DMF. The nanofibers were then carbonized in a tube furnace. Samples were first heated at 1ºC/min ramp rate to 220ºC with 30 min stabilization at 220ºC, followed by 0.33ºC/min ramp rate to 240ºC under oxygen atmosphere. The furnace atmosphere was then switched to nitrogen. The sample was heated at 240ºC in nitrogen for 30 min before ramped up to 900ºC at 5ºC/min rate with 1 hr carbonization time. The CNF/SiNP composites were

characterized by X-ray diffraction (XRD), energy dispersive X-ray spectroscopy (EDX), Raman spectroscopy, scanning electron microscopy (SEM), and transmission electron microscopy (TEM). A three-electrode cell set-up was used to measure galvanostatic charge/discharge characteristics of composite nanofibers at 200 mA/g current density for 20 cycles. Both core-shell and non-core-shell CNF/SiNP after cycling were washed, dried, and examined by SEM.

PANAM/SiNP nanofibers with 15, 30, 50, and 80 wt% Si concentration in the core are denoted here as PANAM/Si-15, PANAM/Si-30, PANAM/Si-50, and PANAM/Si-80, respectively. The pyrolyzed core-shell CNF/SiNP from each is denoted as CNF/Si-15, CNF/Si-30, CNF/Si-50, and CNF/Si-80. The non-core-shell precursor is denoted as n-PANAM/Si and its carbon composite is denoted as n-CNF/Si.

3 Results and Discussions

The presence of Si in the core-shell CNF/Si composites were characterized by XRD, as shown in Fig. 1. The sharp peaks at 28.40º, 47.26º, 56.02º, 68.94º, 76.26º, 87.84º, 94.76º, and 106.44º correspond to (111), (220), (311), (400), (331), (422), (511), and (440) of Si crystal planes, respectively [12]. Because peak intensities correspond to the amount presence of Si, the increase in peak height from pure CNF to CNF/Si-80 indicates the retention of SiNP after pyrolysis. The broad peak at ca. 25º in all samples is the presence of disordered carbon. A sharp peak at 26º is the signature graphite peak [13]. Broadening of this peak implies that electrospun CNF does not contain ordered graphitic carbon crystallite.

SiNP concentrations in carbon was further estimated by EDX and the result is shown in Fig. 2, along with the corresponding I_D/I_G ratio, the intensity of disordered (I_D) and graphitic (I_G) carbon peak characterized by Raman spectroscopy. Lower I_D/I_G ratio is an indication of more ordered graphitic carbon plane and vice versa. It is seen that pure CNF possess the highest I_D/I_G ratio of 1.89 ± 0.09, while all other CNF/SiNP samples possess an I_D/I_G ratio lower than 1.75. I_D/I_G decreases continuously when SiNP concentration in the precursor core increases from 15 to 50 wt%. The increase in graphitic structure with the addition of nanoparticle is a phenomenon called catalytic graphitization. Nanoparticles or inorganic catalysts with an atomic number less than 40 and the first ionic potential between 6 and 8 eV often catalyze the formation of ordered carbon structure at low temperature. At 80 wt% Si, I_D/I_G increases slightly. The reduced graphitic structure might be a result of too much nanoparticle addition and the disruption of graphitic carbon plane. n-CNF/Si possess similar amount of Si concentration and I_D/I_G ratio with CNF/Si-80.

The morphology of carbonized nanofibers were characterized by SEM and TEM. Fibers from all precursors retained their morphology without significant breakage or fusion. For the core-shell CNF/SiNP, SEM and TEM of only CNF/Si-80 are shown in Fig. 3 and Fig. 4, respectively. The average fiber diameter of CNF/Si-80 is $8.1\pm1.5\times10^2$ nm and the brighter spots in Fig. 3 are the presence of SiNP. Although a small amount of nanoparticles emerged onto the surface of CNF, most were embedded homogeneously within the CNF, with a fairly thin layer of CNF, estimated 50 nm, covering the surface of SiNP, as shown in Fig. 4. Because most SiNP were located within the CNF, it was difficult to observe the boundary between individual nanoparticles. The estimated average size for SiNP is 100 nm in diameter. A significant increase in nanoparticle density was observed as the concentration of SiNP increased during electrospinning. Fig. 5 and Fig. 6 are SEM and TEM, respectively, of n-CNF/Si. n-CNF/Si obtains an average fiber diameter of $4.9\pm1.3\times10^2$ nm and a rougher fiber surface with the presence of SiNP granules. The surface agglomerated SiNP is clearly seen in Fig. 6, which shows the different surface morphology from CNF/Si-80. Fig. 7 is the SEM of pure CNF. It possesses a smooth surface with an average fiber diameter of $4.0\pm0.5\times10^2$ nm.

CNF/Si-80, n-CNF/Si, and pure CNF were cycled at 200 mA/g rate for 20 cycles. Both CNF/Si-80 and n-CNF/Si possess an initial Coulombic efficiency of ca. 55 %, which are higher than 32 % of pure CNF. This initial high irreversible capacity was mainly due to the decomposition of electrolyte solution at the carbon surface to form a stable solid electrolyte interface (SEI), which is permeable to Li ions only and protects carbon from further solution decomposition and

degradation of carbon structure. Since the amount carbon proportion is smaller in the CNF/SiNP composite, both CNF/Si-80 and n-CNF/Si possess higher initial Coulombic efficiencies than CNF due to a smaller amount of electrolyte decomposition. The efficiency for all samples recovered to 80 – 90 % for subsequent cycles. The discharge capacity of all samples were summarized in Fig. 8. The highest discharge capacity for CNF/Si-80 and n-CNF/Si were 1094 and 1009 mAh/g, which occurred at the 1st and 2nd cycle, respectively. The capacity of CNF/Si-80 remained fairly stable throughout cycles and the capacity retention after 20 cycles was 72 %. In contrast, the capacity of n-CNF/Si was stable at first 5 cycles but was followed by constant losses afterwards. Its capacity retention after 20 cycles were only 59 %.

In order to investigate the capacity retention of pure SiNP, its capacity was obtained by subtracting CNF/Si-80 or n-CNF/Si capacity with that of pure CNF. The result is summarized in Fig. 9. It is seen that SiNP contributed a total of ca. 700 mAh/g capacity to the nano-composite. The capacity of SiNP from CNF/Si-80 is very stable throughout cycles with insignificant capacity reduction. The capacity reduction of CNF/Si-80 therefore is mainly a result of capacity reduction from CNF. In contrast, the capacity of SiNP from n-CNF/Si first increased from ca. 550 to 700 mAh/g for the first 5 cycles, followed by constant decrease in the subsequent cycles and reached 480 mAh/g at 20th cycle.

CNF/Si-80, n-CNF/Si, and CNF after cycling were examined by SEM and the images are shown in Fig. 10 – Fig. 12. For both CNF/Si-80 and n-CNF/Si, after cycling, fibers were swollen approximately 2× larger. This is mainly due to the expansion of SiNP after alloying with Li ions. The breakage of fibers were a result of Si expansion and contraction during charge and discharge, which exerts mechanical stress on the supporting carbon matrix. However, as seen in Fig. 10, although fibers increased in diameter, they still remained a discrete fibrous structure. Fig. 11, the non-core-shell fiber, does not have a distinct fiber boundary. Fibers appear to fuse together with the swollen surface granules, which are swollen SiNP. This morphology difference can be correlated to the capacity retention behavior of both samples. Carbon coating of CNF/Si-80 prevents SiNP fusion and detachment from the carbon matrix during cycling, therefore retains the reactivity of SiNP. In contrast, n-CNF/Si exposes SiNP on the fiber surface, which often causes nanoparticle fusion, pulverization, detachment from carbon, and eventually loss of Si capacity. Ji *et al.* have demonstrated a similar effect [6]. Fig. 12, the SEM of pure CNF after cycling, shows the swollen average fiber diameter to be 7.4± 1.1×10^2 nm. The smooth fiber surface and intact structure further contrast the effect of SiNP loading on the overall fiber morphology.

4 Conclusions

SiNP loading at ca. 30 wt% has significantly increased the overall capacity of CNF/SiNP composite to ca. 1000 mAh/g. Among all, core-shell structured CNF/SiNP composite has shown enhanced capacity retention of SiNP by a surface carbon coating, which prevents nanoparticle agglomeration upon alloying with Li ions. In order to characterize the stability of the electrode, galvanostatic cycling of the electrode at lower and higher rates will be conducted. Pure carbon samples at corresponding rates will also be conducted to further investigate the causes for capacity fading.

5 Acknowledgement

This work is supported by NSERC through an Exploratory Research Grant. Partial support by AOARD is appreciated. The equipment used in this research is funded by CFI.

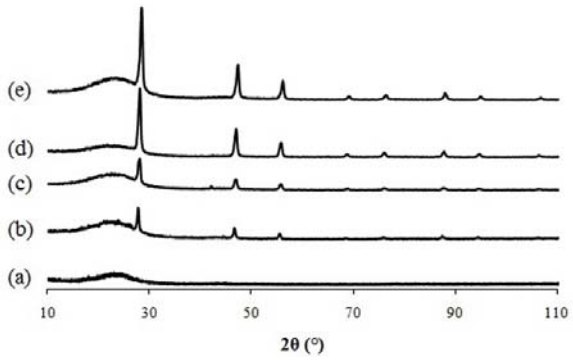

Fig. 1. XRD of pure CNF (a), CNF/Si-15 (b), CNF/Si-30 (c), CNF/Si-50 (d), and CNF/Si-80 (e).

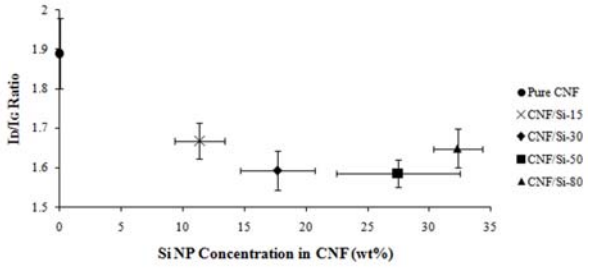

Fig. 2. Raman I_D/I_G ratios of different CNF composite samples vs. their corresponding SiNP concentrations.

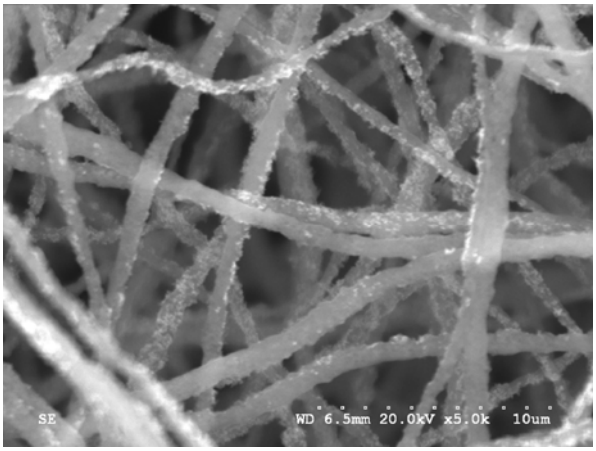

Fig. 3. SEM of CNF/Si-80.

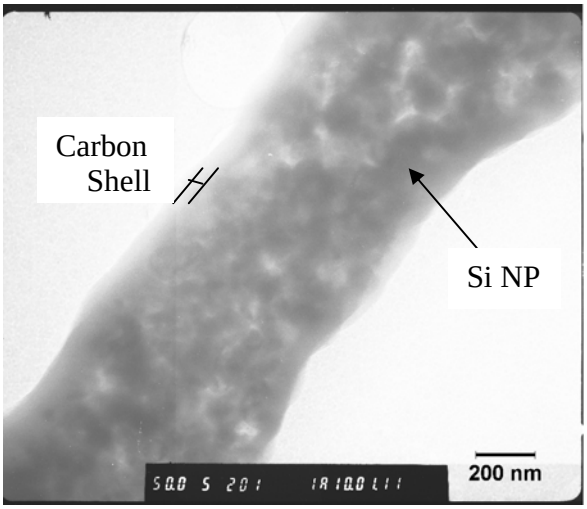

Fig. 4. TEM of CNF/Si-80.

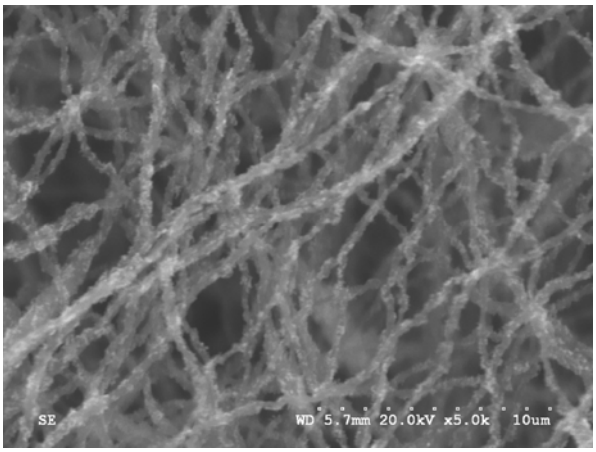

Fig. 5. SEM of n-CNF/Si.

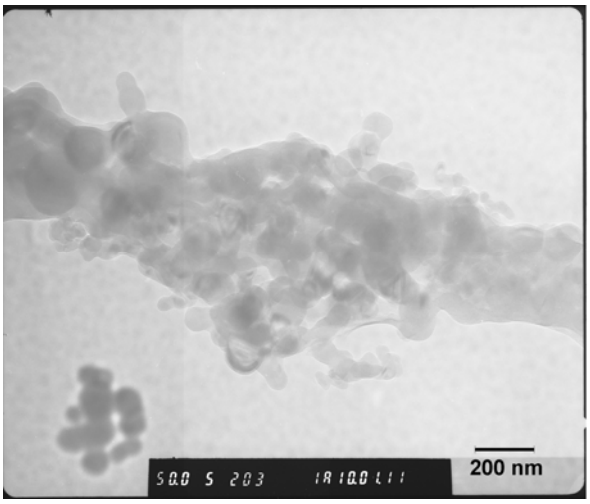

Fig. 6. TEM of n-CNF/Si.

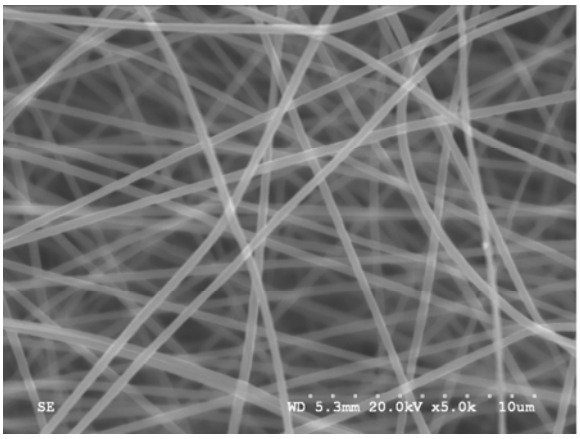

Fig. 7. SEM of pure CNF.

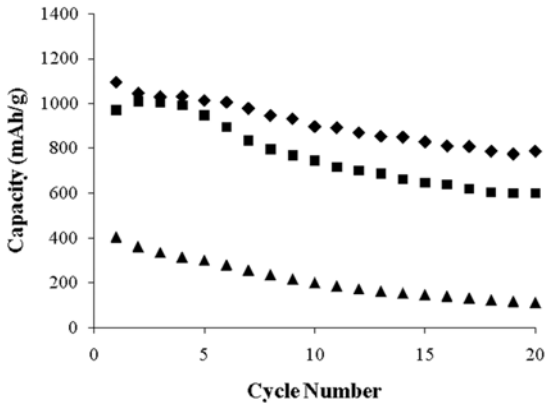

Fig. 8. Discharge capacity summary of CNF/Si-80 (rhombus), n-CNF/Si (square), and pure CNF (triangle).

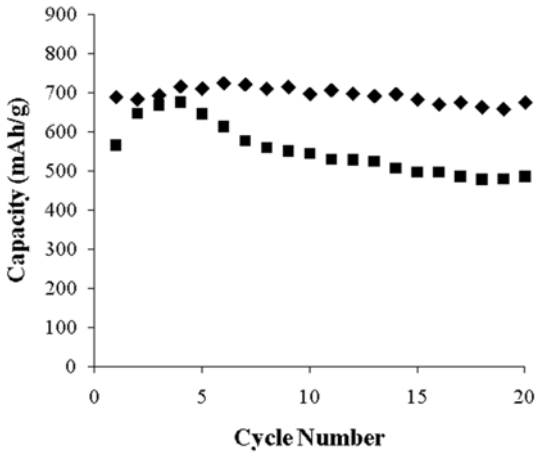

Fig. 9. Discharge capacity of pure SiNP from CNF/Si-80 (rhombus) and n-CNF/Si (square).

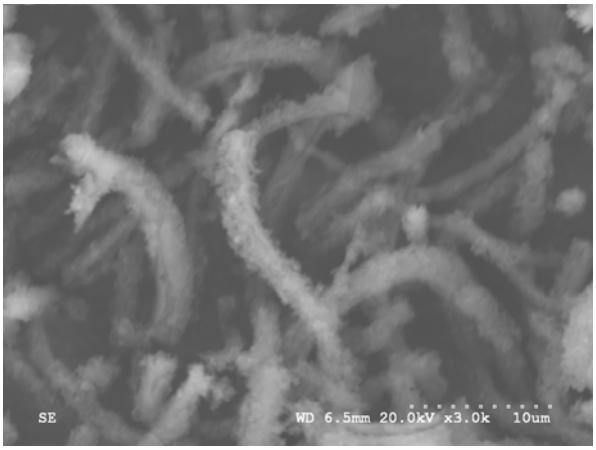

Fig. 10. SEM of CNF/Si-80 after 20 galvanostatic cycles.

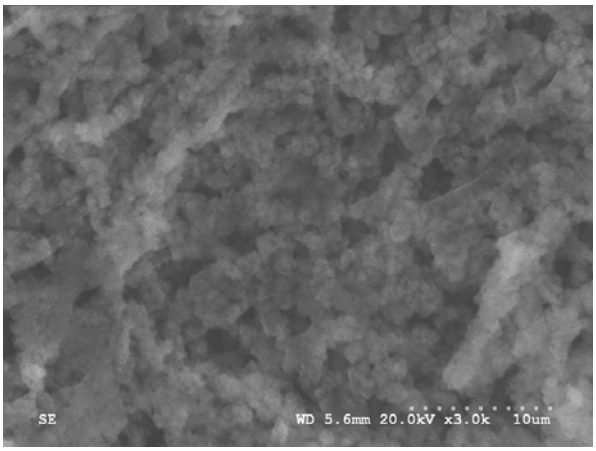

Fig. 11. SEM of n-CNF/Si after 20 galvanostatic cycles.

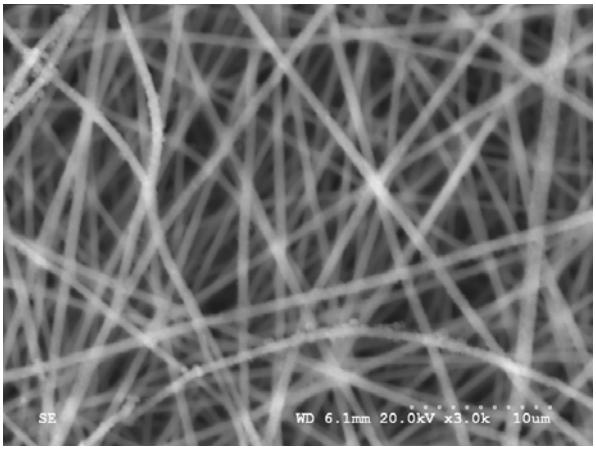

Fig. 12. SEM of pure CNF after 20 galvanostatic cycles.

6 References

[1] R. Teki, M. K. Datta, R. Krishnan, *et al.* "Nanostructured silicon anodes for lithium ion rechargeable batteries". *Small*, Vol. 5, No. 20, pp 2236-2242, 2009.

[2] J. R. Dahn, T. Zheng, Y. Liu, *et al*. "Mechanisms for lithium insertion in carbonaceous materials". *Science*, Vol. 270, No. 5236, pp590-593, 1995.

[3] M. Endo, C. Kim, K. Nishimura, *et al*. "Recent development of carbon materials for Li ion batteries". *Carbon*, Vol. 38, No. 2, pp 183-197, 2000.

[4] S. Hang "Coke vs. graphite as anodes for lithium-ion batteries" . *Journal of Power Sources*, Vol. 75, No. 1, pp 64-72, 1998.

[5] T. Nagura and K. Tozawa. "Lithium ion rechargeable battery". *Progress Batteries and Solar Cells*, Vol. 9, pp209-216, 1990.

[6] L. Ji and X. Zhang "Electrospun carbon nanofibers containing silicon particles as an energy storage medium". *Carbon*, Vol. 47, No. 14, pp 3219-3226, 2009.

[7] U. Kasavajjula, C. Wang, J. Appleby "Nano- and bulk-silicon-based insertion anodes for lithium-ion secondary cells". *Journal of Power Sources*, Vol. 163, No.2, pp1003-1039, 2007.

[8] B. A. Boukamp, G. C. Lesh, R. A. Huggins, "All-Solid Lithium Electrodes with Mixed-Conductor Matrix". *Journal of the Electrochemical Society*, Vol. 128, No. 4, pp725-729, 1981.

[9] H. Li, X. Huang, L. Chen, *et al*. "A high capacity nano-si composite anode material for lithium rechargeable batteries". *Electrochemical and Solid-State Letters*, Vol. 2, No. 11, pp 547-549, 1999.

[10] L. Cui, R. Ruffo, C. K. Chan, *et al*. "Crystalline-amorphous core-shell silicon nanowires for high capacity and high current battery electrodes". *Nano Letters*, Vol. 9, No. 1, pp 491-495, 2009.

[11] P. Gao, J. Fu, J. Yang, *et al*. "Microporous carbon coated silicon core-shell nanocomposite via in situ polymerization for advanced Li-ion battery material". *Physical Chemistry Chemical Physics*, Vol. 11, No. 47, pp11101-11105, 2009.

[12] D. P. Yu, Z. G. Bai, Y. Ding, *et al*. "Nanoscale silicon wires synthesized using simple physical evaporation". *Applied Physics Letters*, Vol. 72, No. 26, 3458-3461, 1998.

[13] C. Kim, S. Park, J. Cho, *et al*. "Raman spectroscopic evaluation of polyacrylonitrile-based carbon nanofibers prepared by electrospinning". *Journal of Raman Spectroscopy*, Vol. 35, No. 11, pp928-933, 2004.